Journal of Hydroscience and Hydraulic Engineering
Vol. 22, No.1 May, 2004, 37-50

SPATIAL CORRELATION STRUCTURES OF WATER SURFACE FLUCTUATION WITH TURBULENCE IN OPEN-CHANNEL FLOWS

By

Hitoshi Miyamoto

Department of Architecture and Civil Engineering, Kobe University,
Rokkodai 1-1, Nada, Kobe 657-8501, Japan

and

Kenji Shimoyama

Graduate Student, Graduate School of Science and Technology, Kobe University,
Present address: NEWJEC Co., Ltd., Shima-no-uchi 1-20-19, Chuo, Osaka 542-0082, Japan

SYNOPSIS

Laboratory experiments were conducted to investigate interactions between the water surface fluctuations and turbulence structures in open-channel flows. Instantaneous velocity vectors and the corresponding water surface profiles were measured by a simultaneous image measurement method. The proper orthogonal decomposition (POD) of the water surface fluctuations successfully detected their predominant spatial fluctuation patterns, most of which represented sinusoidal wave shapes. By using the modal amplitudes of the POD eigenvectors, we calculated spatial correlation coefficients between the amplitudes and the velocity fluctuations. The result showed that there existed a thin surface-influence-layer near the water surface in which the turbulent flow seemed to be parallel to the wavy surface and also that there was the specific interaction between the water surface fluctuations and the large-scale turbulence structures that have the same longitudinal scale. Furthermore, it was revealed that the spectral distribution of water surface fluctuations followed the –10/3 power of the wave-number.

INTRODUCTION

Understanding and evaluating the roles of turbulent flows around the free water surface have become increasingly important from the perspective of environmental fluid mechanics and engineering because turbulence structures near the surface regions may influence considerably free surface phenomena such as momentum exchanges, gas transfer, self aeration etc. which are primarily essential to aquatic life and its environment. In the present study, laboratory experiments were conducted to

investigate fluctuation characteristics of the water surface and their relations to turbulence structures in open-channel flows. A simultaneous image measurement method recently proposed by Miyamoto et al. (2) was used to quantify instantaneous velocity vectors and the corresponding water surface profile in a vertical cross section of the open-channel flows. The proper orthogonal decomposition (POD) (see e.g. Berkooz et al. (1)) was applied to the measurement data of the water surface fluctuations in order to extract their predominant fluctuation patterns. Interactions between the water surface fluctuations and the turbulence structures were examined by calculating space correlations of the POD predominant fluctuations with the turbulence in the open-channel flow. Moreover, based on the findings obtained above, the wave-number spectrum of water surface fluctuations was discussed in some detail.

Although there have been many research works on the topic of turbulent flows with a free surface boundary, we have had little knowledge about the relationships between the surface fluctuations and the turbulence structures, in particular, when a Froude number becomes large and the surface fluctuations are considerably pronounced. As for the recent experimental works on the turbulent open-channel flows with relatively high Froude numbers, Nezu & Nakayama (5), (6) measured the turbulence and the water surface fluctuations by using a laser Doppler anemometer (LDA) and an ultra-sonic displacement sensor. They reported that the turbulence structures of open-channel flows in near surface region differed much from those of pipe flows through the examination of turbulence statistics and its energy budget (6), and that by using a space-time correlation analysis there might exist a relationship between coherent vortex in the wall region and those in the near surface region (5). Their discussion was mainly focused on how turbulence characteristics changed when turbulence came up from the wall region toward the free surface since the data of water surface fluctuations were restricted at only one measurement point.

As for numerical studies there have also been many articles on turbulent free surface flows. Among these works it was considerable that Shen et al. (7) confirmed that there existed two layers in near surface region, namely, a 'surface layer' and a 'blockage layer' by performing the direct numerical simulation (DNS) of a turbulent free surface flow with a small Froude number. The surface layer represented a thin free surface viscous boundary layer, while the blockage layer was a relatively thicker one in which the turbulent flows were changed to satisfy with the kinematic boundary condition at the free surface. Moreover, the recent DNS study on turbulent open-channel flows by Yokojima & Nakayama (8) indicated that turbulence structures in a near surface region had three-dimensional characteristics as the Froude number became larger. However, since these numerical results were obtained from linearized boundary conditions such as the small amplitude wave approximation, verification based on the appropriate experimental works is necessary in order to elucidate the phenomena of turbulent free surface flows.

In this study, we could detect the predominant fluctuation characteristics of the water surface profiles from the experimental data of the simultaneous image measurements. Therefore, we investigated the 'free surface – turbulence structures' interactions from a viewpoint of the velocity fluctuations originated from the predominant water surface fluctuations, instead of the conventional viewpoint of the wall turbulence reaching toward the water surface. Although it was recognized that the conventional viewpoint was of importance because the wall boundary generated and maintained turbulence in open-channel flows, it also seemed to be obvious that this kind of different viewpoint with the new measurements must be necessary for further understanding of the phenomena.

Table 1 Overview of hydraulic conditions

Case	Q (cm^3/s)	B (cm)	H (cm)	$\overline{U}$ (cm/s)	U_* (cm/s)	$1/I$	Re ($\times 10^4$)	Re_*	Fr
1	2.5 $\times 10^3$	25	3.29	30.4	1.53	1149	1.0	502	0.53
2			2.91	34.3	1.78	747	1.0	518	0.64
3			2.42	41.3	2.14	447	1.0	517	0.85
4			1.89	52.8	2.67	237	1.0	505	1.23

Q: flow rate, B: channel width, H: mean water depth, $\overline{U}$: mean bulk velocity, U_* : friction velocity, I : channel slope, $Re = \overline{U}\,H / \nu$: Reynolds number based on $\overline{U}$ and H, $Re_* = U_* H / \nu$: Reynolds number based on U_* and H, $Fr = \overline{U} / (gH)^{1/2}$: Froude number.

HYDRAULIC EXPERIMENTS AND SIMULTANEOUS IMAGE MEASUREMENTS

Experimental Conditions

The laboratory experiments reported here were conducted in a clear acrylic flume with length of 10 m and width B = 25 cm. The hydraulic conditions are listed in Table 1. In the experiments, we kept a Reynolds number based on the mean bulk velocity $\overline{U}$ and the mean water depth H with the water viscosity ν, $Re = \overline{U}H/\nu$, a constant (= 1.0×10^4), whereas we changed a Froude number based on $\overline{U}$ and H with the gravitational acceleration g, $Fr = \overline{U}/\sqrt{gH}$, from 0.53 (subcritical flow) to 1.23 (supercritical flow), as indicated in Table 1. We also kept an aspect ratio of channel B/H greater than 7.0 throughout the experiments so that we could obtain the two-dimensional flow characteristics in long-term turbulent structures in the central zone of the channel, where effects of the side-wall friction almost disappears (see Nezu and Nakagawa (4)). As for the mean velocity, since the values of a Reynolds number based on the friction velocity U_* and H, $Re_* = U_* H / \nu$, were set to be about 500 in all cases, the vertical distributions obtained here were recognized to be good agreement with the well-known log-law distribution, more precisely, with the log-wake law distribution with almost zero wake function (see Nezu and Nakagawa (4)). Consequently, the dependence of the Froude number on turbulence characteristics in the open-channel flows was expected to be investigated without any differences in the mean velocity structures throughout the experiments.

Simultaneous Image Measurements of Velocity Field and Water Surface Profile

Figure 1 shows a schematic view of the image measurement system used in the laboratory experiments. The image measurement system was composed of several pieces of equipment, i.e., a double pulse YAG laser with a laser beam expander, a high-resolution CCD camera, a mirror, monitors, a timing controller, and a personal computer with a hard disk. Particles with diameters of about 0.02 mm and with a specific gravity of 1.02 were utilized as a tracer for visualization. A flow field, where the tracer particles were seeded, was visualized by a laser light sheet, as shown in Fig. 1. The visualized images were captured by the high-resolution CCD camera with 1008×1018 pixels and were recorded on the hard disk in the PC. An image of the water-surface profile, on the other hand, was taken through the mirror so that the water surface would not be hidden by a meniscus of a water surface on the front wall. Consequently, the images of both the flow field and the water surface

profile on the vertical laser light plane were simultaneously obtained in the same image flame. Figure 2 shows an example of the visualized images. The upper part in the Fig.2 shows the image of the water surface profile through the mirror, while the lower part shows the image of the flow field. An image processing technique proposed by Miyamoto et al. (2) was applied to the images in order to simultaneously quantify instantaneous water surface profiles and velocity vectors. In the image processing technique, an edge extracting algorism is employed to detect the location of water surface, while a particle image velocimetry (PIV) is applied to measure the velocity vectors (Miyamoto et al. (2)). The measurement section in the experiments was a vertical cross section along the streamwise axis at the center of channel width, and was located at about 7.5 – 8.0 m downstream part from the entrance of the flume where the turbulent boundary layer generated on the bottom wall was supposed to be fully developed. In the image measurements the sampling interval of velocity vectors (temporal resolution) was 1/15 seconds and the pixel size of the image (spatial resolution) was about 0.098 mm.

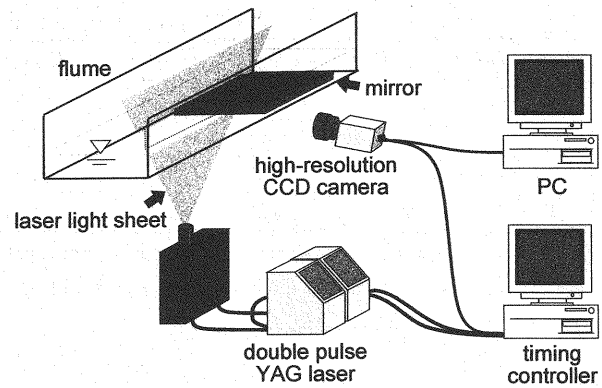

Fig.1 Schematic of image measurement system

As for the reference frame employed in this study, x, y in the Cartesian coordinate denote the streamwise direction (positive downward) and the vertical direction (positive upward), respectively, with the origin at a point on the channel bed. U, V denote the components of mean velocity in the x-, y- directions, respectively, u, v, the instantaneous velocities, and u', v', the velocity fluctuations. h represents the instantaneous water surface profile, while H and h' are the mean and fluctuation components of the water surface profile.

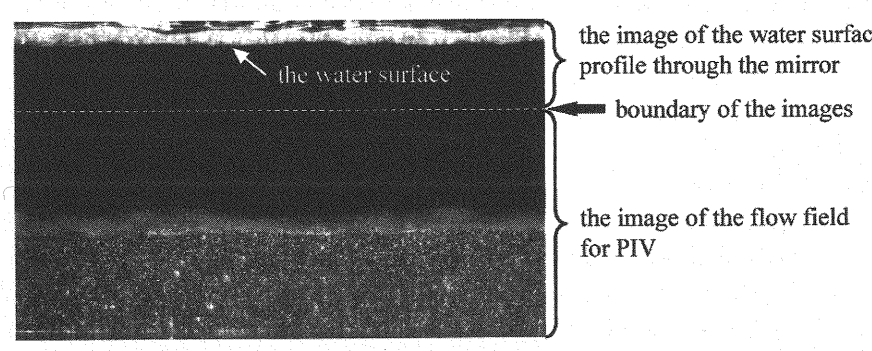

Fig.2 An example of the visualized images with the explanation

ANALYTICAL METHODS

In this study, we used the proper orthogonal decomposition (POD) (see e.g. Berkooz et al. (1)) to extract fluctuation characteristics of the water surface and also applied the space correlation analysis to investigate interactions between water surface fluctuations and turbulence structures. The two analytical methods are briefly summarized below.

Proper Orthogonal Decomposition

The POD provides an efficient basis for the modal decomposition of an ensemble of data by analyzing the data as an eigenvalue problem. In the present paper, the POD was applied to the water surface fluctuations h'.

The eigenvectors φ_m in the POD are obtained from the following equation.

$$[\mathbf{R}_h]\{\varphi_m\} = \lambda_m\{\varphi_m\} \tag{1}$$

where

$$[\boldsymbol{R}_h]=[\boldsymbol{R}_{i,j}]=\left[\frac{1}{M}\sum_{p=1}^{M} h'(x_i,t_p)h'(x_j,t_p)\right], \qquad i, j = 1, 2, \ldots, N \tag{2}$$

is the covariance matrix of the water surface fluctuations h', m represents the number of the POD mode, and λ_m represents the eigenvalue in mode m. In Eq. (2), x_i denotes the locations of each measurement point in the x-direction, N, total number of the measurement points, t_p, each discrete time, and M, total number of the discrete times. Since the eigenvectors φ_m form a complete orthogonal set, the water surface fluctuation h' is reproduced by the following equation.

$$h'(x_i, t_p) = \sum_{m=1}^{N} h'_m(x_i, t_p) = \sum_{m=1}^{N} a_m(t_p)\,\varphi_m(x_i) \tag{3}$$

where

$$a_m(t_p) = \langle h'(x_i, t_p)|\varphi_m(x_i)\rangle / \langle \varphi_m(x_i)|\varphi_m(x_i)\rangle \tag{4}$$

is the modal amplitude (modal time-series) and h'_m is the component of h' in mode m. In addition, since the eigenvalue λ_m corresponds to the square of fluctuation intensity of the h'_m, a cumulative contribution ratio C_m is given with the eigenvalues by using the following equation:

$$C_m = \sum_{n=1}^{m} r_n = \sum_{n=1}^{m} \frac{\lambda_n}{\sum_{l=1}^{N} \lambda_l} \tag{5}$$

where r_n is the contribution ratio in each mode n.

Space Correlation Analysis

A space correlation coefficient $COR_{fg}(x, y)$ of fluctuations $f(t_p)$ and $g(x, y, t_p)$ are defined as follows.

$$COR_{fg}(x,y)=\frac{\sum_{p=1}^{M} f(t_p)\,g(x,y,t_p)}{(\sum_{p=1}^{M} f(t_p)^2)^{1/2}\cdot(\sum_{p=1}^{M} g(x,y,t_p)^2)^{1/2}} \tag{6}$$

In this study, as will be discussed in the next chapter, the modal amplitude a_m of the water surface fluctuation h'_m (see Eq. (4)) was chosen to calculate the correlation coefficients, instead of the water surface fluctuation h' itself.

RESULTS AND DISCUSSION

Instantaneous Velocity Field and Turbulence Statistics

An instantaneous velocity vectors (u, v) and the corresponding water surface profile h are shown in Fig. 3 (Case 4: Fr = 1.23). From Fig. 3(a) the values of h are almost constant along the streamwise direction, but its shape seems to have small wavy fluctuations with wavelengths of 3 – 4 cm. Furthermore, at this instant the values of h throughout the profile become smaller than the mean water surface H = 1.89 cm (see Table 1, Case 4). In the instantaneous velocity vector field shown in Fig. 3(b), there are the several regions in each of which the velocity vectors fluctuate either upward or downward, e.g. (x = 6 – 8 cm, y = 1 – 1.7 cm).

Figures 4 and 5 show the distributions of mean velocity U^+ and those of turbulent intensities $\sqrt{\overline{u'^2}}/U_*$, $\sqrt{\overline{v'^2}}/U_*$ respectively.

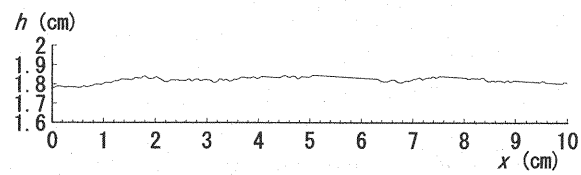

(a) A water surface profile

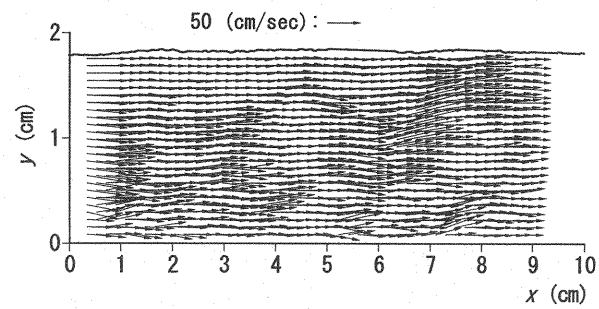

(b) Velocity vectors and the water surface profile

Fig.3 A snapshot of instantaneous velocity vectors and the corresponding water surface profile. The water surface profiles in (a) and (b) are the same. The simultaneous image measurement method was used to obtain the data. Case 4: Re_* = 505, Fr = 1.23.

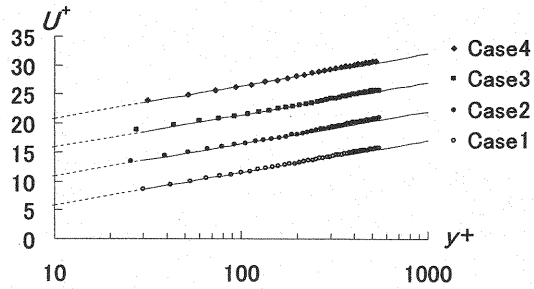

Fig.4 Distributions of the mean velocity U^+. The experimental values are compared with the log-law curve. The vertical axis in the figure is shifted for the comparison between the cases.

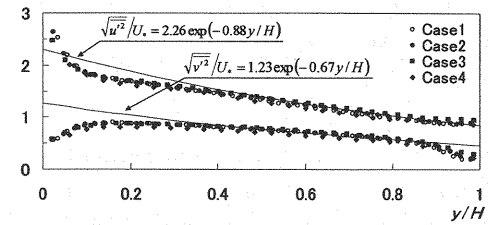

Fig.5 Distributions of turbulent intensities $\sqrt{\overline{u'^2}}/U_*$ and $\sqrt{\overline{v'^2}}/U_*$. The experimental values are compared with the semi-theoretical curves (Nezu et al. (4)).

The values of the friction velocity U_* listed in Table 1 were calculated by matching the velocity data to the log-law with the Karman constant κ = 0.41. The experimental values of U^+ are in very good agreement with the calculated curves of the log-law. As expected earlier, no precise wake regions exist near the water surface due to the $Re_* \approx$ 500, which results in no significant difference in the mean velocity structures throughout all cases of the experiments. With respect to the turbulence intensities shown in Fig. 5, the experimental values of both $\sqrt{\overline{u'^2}}/U_*$ and $\sqrt{\overline{v'^2}}/U_*$ agree well with the semi-theoretical curves by Nezu et al. (see Nezu & Nakagawa (4)). In addition, the values of $\sqrt{\overline{v'^2}}/U_*$ decrease sharply near the surface region about $y/H > 0.8$ as the free surface is approached, which seems to be the effects due to the kinematic boundary condition at the water surface like the blockage effect by Shen et al. (7). Consequently, it is verified from these results that the velocity vectors with high accuracy are obtained by the simultaneous image measurements.

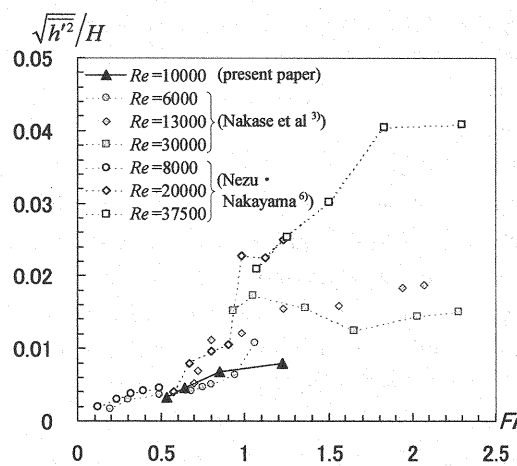

Fig.6 Relationship between the intensity of water-surface fluctuation $\sqrt{\overline{h'^2}}/H$ and the Froude number Fr.

Figure 6 shows the relationship between the intensity of water surface fluctuations $\sqrt{\overline{h'^2}}/H$ and the Froude number Fr. The values of $\sqrt{\overline{h'^2}}/H$ in the present study (symbols: ▲) become large as Fr increases. This increasing feature with Fr is almost the same as the results of other experiments by Nakase et al. (3), as indicated in Fig. 6. However, a sharp increase around the critical flow (Fr = 1) reported by Nezu & Nakayama (6) does not appear in this study. Since the data by Nakase et al. (3) also do not have the sharp increase (e.g., symbols: ▒), with respect to the fluctuation characteristics of water surface it should be necessary to take the different approaches through which the interactions of water surface fluctuations with turbulence structures beneath the surface can be

considered.

Fluctuation Characteristics of Water Surface Profile

The water surface fluctuations are supposed to reflect somehow the turbulence structures with various spatiotemporal scales. Therefore, before investigating their interactions, we made an effort to detect predominant fluctuation characteristics of the water surface by applying the POD analysis to the water surface fluctuations $h'(x, t)$.

Figure 7 shows the distributions of the POD eigenvectors φ_m of surface fluctuation h' obtained by Eq. (1) (Case 1: Fr = 0.53). The cumulative contribution ratio C_m indicated at the right side of each figure shows that 90 % of the water fluctuations are reproduced by summing up φ_m from mode m= 1 to 7. Predominant patterns of the water surface fluctuations represented by φ_m are almost the same as sinusoidal waves, and the values of their wave-number increase as the number of the POD mode m becomes large. Furthermore, these kinds of sinusoidal distributions continue to appear in φ_m with higher POD modes. This result reveals that fluctuation distribution of the water surface is almost completely represented by the superposition of sinusoidal waves in this case (Case 1: Fr = 0.53). The nonlinear behavior of the water surface fluctuations, on the other hand, is reflected by the modal amplitudes a_m (see Eqs. (3) and (4)).

Figure 8 shows the distributions of eigenvectors φ_m in the first mode for all cases (m = 1, Case 1-4: Fr = 0.53-1.23). The distribution of φ_m changes from a sinusoidal wave to nearly a constant as the Froude number Fr increases. This indicates that at a supercritical flow condition (Fr > 1.0

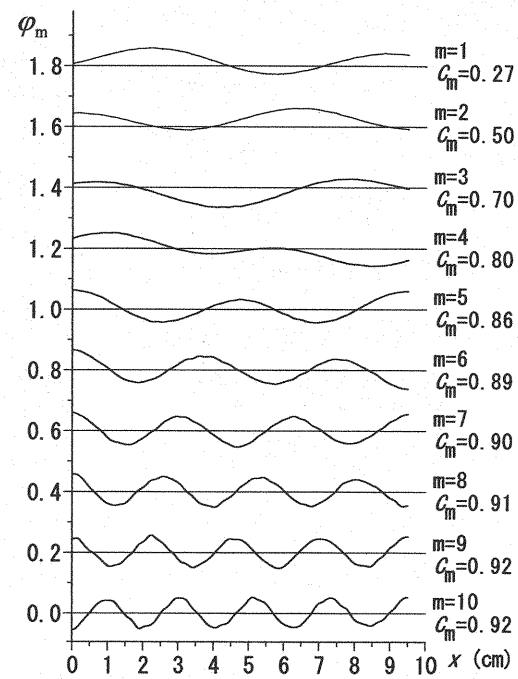

Fig.7 Eigenvectors φ_m of the water surface fluctuations h' (m denotes the number of the POD mode). The vertical axis is shifted in 0.2 between two successive modes, m and m+1, in order to compare wavelengths among the modes. Case 1: Fr = 0.53.

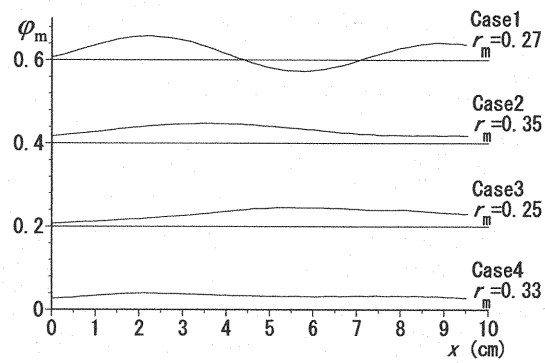

Fig.8 Comparison of the first mode eigenvectors φ_m (m = 1) of the water surface fluctuations in all cases. The Froude number Fr is varied from 0.53 to 1.23. The vertical axis is shifted in 0.2 between two successive cases.

but not so high values) the fluctuation component that has a larger streamwise scale becomes predominant rather than the component with a sinusoidal shape. This large-scale fluctuation component might be generated by different factors from the turbulence structures beneath the surface whose distinct correlations with the sinusoidal-shaped components will be revealed in the next section. Furthermore, in higher POD modes m ≥ 2, 3, … in Case 2-4 the distributions of φ_m become sinusoidal shapes, which is the same feature as in Case 1.

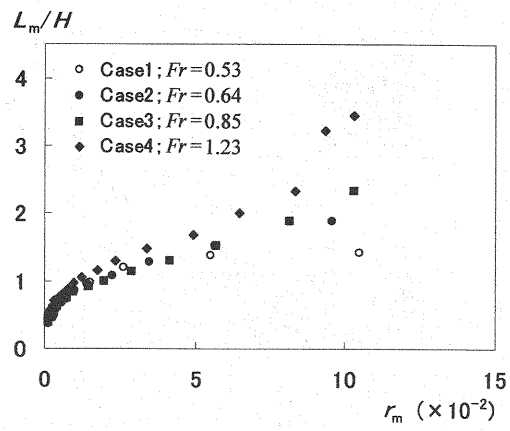

Fig.9 Relationship between non-dimensional wavelengths L_m/H of the eigenvectors and their contribution ratios r_m.

With respect to φ_m with the sinusoidal wave distributions (i.e., most of the φ_m's) we calculate the corresponding wavelengths L_m. Figure 9 shows the relationship between the non-dimensional wavelength L_m/H and the contribution ratio r_m. Here, r_m represents the ratio of the square of the water surface fluctuation $\overline{h'^2_m}$ in the mode m to that of the whole fluctuation $\overline{h'^2}$, as explained in the previous chapter. In Fig. 9 there exists a strong interrelation between L_m/H and r_m, which means that the water surface fluctuation with a longer spatial scale has larger fluctuation intensity. Moreover, it should be noted that there is no Froude number dependence in $L_m/H < 2$. This result indicates that when the wavelength L_m smaller than $2H$, the predominant components with the same streamwise spatial scale have the same ratio of the fluctuation intensity to the total intensity $\overline{h'^2}$ irrespective of the Froude number Fr. In $L_m/H > 2$ of Fig. 9, on the other hand, the values of L_m/H with same r_m increase as Fr becomes larger. Therefore, it is found that the Froude number dependence of the water surface fluctuation h' appears at the fluctuations with the streamwise scale larger than $2H$.

Spatial Correlations of Water Surface Fluctuations and Turbulence

To examine the interactions between the water surface fluctuations and turbulence structures beneath the surface, we calculated their space correlation coefficients with Eq. (6). In this study, since we could not obtain distinct correlation structures between the water surface fluctuation h' at one measurement point and the velocity fluctuations u', v', we carried out a conditional space correlation analysis; namely, by utilizing the fact that $h'(x, t)$ is represented by the superposition of the eigenvectors φ_m, we calculated the space correlation coefficients $COR_{amu'}$, $COR_{amv'}$ between the modal amplitude a_m of the fluctuation h'_m and u', v' (see Eqs. (3) and (4)).

Figure 10 shows the contours maps of $COR_{amu'}$, $COR_{amv'}$ (Case 4: Fr = 1.23, mode m = 3,7,10). The corresponding eigenvectors φ_m have the sinusoidal wave shapes that are drawn in the upside of each figure. The distributions of $COR_{amv'}$ in Fig 10(a-2), (b-2), (c-2) have positive and negative regions alternately along the streamwise direction both in near surface region (about $y/H >$

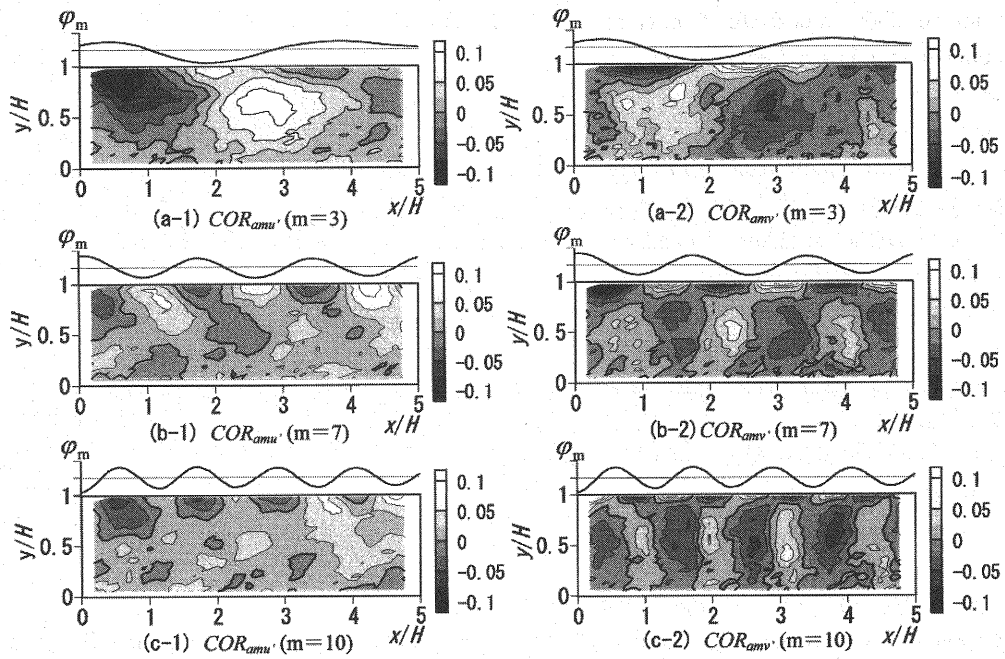

Fig.10 Spatial correlation coefficients of the modal amplitude a_m of the surface fluctuation component h'_m and the velocity fluctuation components u' and v'. The figures in left column show the distributions of the coefficients between a_m and u', while those in right show those between a_m and v', in modes m = 3,7,10, Case 4: Fr = 1.23. The profile of the corresponding eigenvector is indicated in the upside of the each figure.

0.8) and in central region of the flow (about $y/H < 0.8$), and their spatial scales are the same as the wavelengths L_m of the corresponding eigenvectors φ_m. Therefore, it is revealed that the turbulence structures beneath the water surface can be divided into two layers, namely, the layer near the surface with thickness about $\delta = 0.2H$ where the turbulence is strongly affected by the water surface fluctuations and the layer under the surface influence layer where large-scale turbulent motions are well developed. This thickness δ is almost the same scale as that by Nezu & Nakayama (6). We call this thin layer near the surface the surface-influence-layer hereafter in this paper. The distributions of $COR_{amu'}$ in Fig 10(a-1), (b-1), (c-1), on the other hand, also have alternate positive and negative regions around the surface, but do not have such regions in the central region of the flow. Moreover, it is shown in the distributions $COR_{amv'}$ in Fig 10(a-2), (b-2), (c-2) that, in the upper part of the surface-influence-layer, the values of $COR_{amv'}$ become positive where the shapes of the φ_m changes from troughs to crests, while the values become negative from crests to troughs. This result implies that the turbulent flow in the upper region of the surface-influence-layer becomes parallel to the wavy surface due to the kinematic boundary condition at the surface. From these discussions, we can conclude that the surface-influence-layer obtained here is supposed to be almost the same as the blockage layer by Shen et al. (7). The distributions of $COR_{amv'}$ show that, in the central region of the flow, the values of $COR_{amv'}$ become positive where the corresponding shapes of the φ_m

changes from crests to troughs, and vice versa. It is confirmed from this evidence that there is a specific interaction among the surface fluctuation h'_m, the turbulence in the surface-influence-layer, and the large-scale turbulence structure in the central region of the flow that have the same spatial scale in the streamwise direction. Furthermore, from the fact that the characteristics of the space correlation structures obtained here are almost identical for the eigenvectors φ_m having sinusoidal shapes, this type of 'surface fluctuations – large-scale turbulence structures' interactions is expected to be universal in turbulent open-channel flows.

As examined earlier in Fig. 8, when the flow becomes supercritical ($Fr > 1.0$), the fluctuation component that has a spatial scale considerably larger than the scale of measurement cross section is most predominant in the water surface fluctuations. In this component (Case 4: $Fr = 1.23$, mode m = 1) there is no specific structure in $COR_{amu'}$ and $COR_{amv'}$. This implies that the detection of the interaction failed due to the lack of the flow field information because the experimental data collected in this study were restricted in the measurement vertical cross section with the streamwise length of about 10 cm. Consequently, further experimental works need to be carried out with respect to the Froude number dependence of the water surface fluctuations.

Wave-Number Spectrum of Water Surface Fluctuations

Based on the discussion already mentioned in the previous two sections of this chapter, we examine the wave-number spectrum of water surface fluctuations.

The POD analysis on the water surface fluctuation in this paper is equivalent to the spectrum analysis since most of the obtained eigenvectors φ_m are sinusoidal waves with the wavelengths L_m. Therefore, the contribution ratio r_m obtained from the POD analysis corresponds to the value of the spectrum at the wave-number $k_m = 2\pi/L_m$ of the streamwise direction. As for the discussion in Fig. 10, on the other hand, it was found that there is a specific interaction between the surface fluctuation h'_m and the large-scale turbulence structure that have the same longitudinal scale L_m. Therefore, if we assume a physical mechanism on which the pressure fluctuation p'_{Lm} due to the large scale turbulence u'_{Lm} with L_m makes the surface fluctuation h'_m with the same scale L_m, we can conjecture that in the Fourier space the $\rho u'^2_{Lm} \sim p'_{Lm} \sim \rho g h'_m$ have the same slope in the spectral distributions. Consequently, when the spectrum of u'_{Lm} follows the well known –5/3 power law, the spectrum of h', which is equivalent to r_m in this study, follows the –10/3 power of the wave-number k_m in the spectral distribution.

Figure 11 shows the spectral distributions of water surface fluctuation h' that are obtained by redrawing the relationship in Fig. 9 on the basis of the above consideration. It is evident in Fig 11 that there exists a range in which the slope of the distribution follows the –10/3 power of the wave-number k_m in each case. In addition, the range with the –10/3 power becomes large as the Froude number Fr increases. In this study, Fr is in proportion to a Fouude number $Fr_* = U_*/\sqrt{gH}$, where the numerator of Fr_* represents the amount of a driving force of the water surface fluctuations because the wall boundary mainly maintains the turbulence structures of the whole open-channel, while the denominator represents the amount of a restoring force due to the gravity. Therefore, the reason for the range enlargement seems to be that the effect of turbulence as the driving force becomes relatively larger as Fr_* (or Fr) increases.

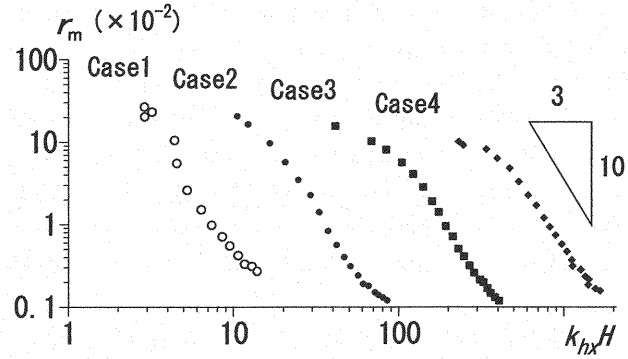

Fig.11 Streamwise spectrum of the water surface fluctuation. The values in horizontal axis are shifted by multiplying $\times 5$, $\times 5^2$, $\times 5^3$ in Case2, 3, 4, respectively, in order to compare the distributions among the cases.

CONCLUSIONS

Laboratory experiments on the turbulent open-channel flows with $Re_* \approx 500$ and $Fr = 0.53$–1.23 were conducted to investigate the interactions between the water surface fluctuations and the turbulence structures beneath the free surface. The simultaneous image measurement method is used to obtain the velocity vectors and the water surface profile, and the POD and the space correlation analyses are applied to examine their interactions. The main conclusions obtained from this study are as follows:

(1) From the results of the POD analysis on the water surface fluctuations, it is shown that most of the predominant fluctuation patterns become sinusoidal wave distributions with certain wavelengths L_m. The Froude number dependence of the surface fluctuations appears obviously in the POD component with the scale L_m larger than twice the mean water depth H.

(2) There exists a layer near the water surface with thickness about $\delta = 0.2H$ where the turbulence is strongly affected by the water surface fluctuations (the surface-influence-layer). In the upper region of the surface-influence-layer, the turbulent flow seems to become parallel to the wavy surface due to the kinematic boundary condition at the surface.

(3) There is a specific interaction between the predominant surface fluctuation, the turbulence in the surface-influence-layer, and the large-scale turbulence structure in the central region of the flow that have the same spatial scale in the streamwise direction.

(4) The spectral distribution of water surface fluctuations follows the –10/3 power of the wave-number. The range with the –10/3 power becomes larger as the Froude number increases.

ACKNOWLEDGEMENTS

Partial Support from the Japan Society for the Promotion of Science (JSPS), Grant-in-Aid for Scientific Research (B)(1)(No.: 14350268, Head Investigator: Prof. K. Michioku of Kobe University) is gratefully acknowledged. We are grateful to the referees for their constructive comments, and to

Mr. Y. Hata, a graduate student at Kobe University, for his help in experiments.

REFERENCES

1. Berkooz, G., P. Holmes, and J.L. Lumley: The proper orthogonal decomposition in the analysis of turbulent flows, Annual Review of Fluid Mechanics, Vol.25, pp.539-575, 1993.
2. Miyamoto, H., T. Kanda, K. Ooe, and K. Shimoyama: Simultaneous measurements of water-surface and velocity using image processing technique and analysis of open-channel flow over concave bed with water-surface fluctuation, Journal of Hydraulic, Coastal and Environmental Engineering, JSCE, No.726/II-62, pp.41-53, 2003 (in Japanese).
3. Nakase, Y., S. Yokojima, A. Nakayama, and I. Fujita: Measurements of surface fluctuations in open-channel turbulent flow using ultra-sonic and laser displacement sensors, Proceedings of 2000 Meeting of Japan Society of Fluid Mechanics, pp.243-244, Kyoto, Japan, 2000 (in Japanese).
4. Nezu, I. and H. Nakagawa: Turbulence in Open-Channel Flows, IAHR-Monograph, A. A. Balkema, Rotterdam, Netherlands, 281pp., 1993.
5. Nezu, I. and T. Nakayama: Space-time correlation structures of coherent vortices near the free surface, Journal of Hydraulic, Coastal and Environmental Engineering, JSCE, No.586/II-42, pp.51-60, 1998 (in Japanese).
6. Nezu, I. and T. Nakayama: Relationship between turbulent structures near the free-surface and surface-wave fluctuations, Journal of Hydraulic, Coastal and Environmental Engineering, JSCE, No.593/II-43, pp.69-78, 1998 (in Japanese).
7. Shen, L., X. Zhang, D.K.P. Yue, and G.S. Triantafyllou: The surface layer for free-surface turbulent flow, Journal of Fluid Mechanics, Vol.386, pp.167-212, 1999.
8. Yokojima, S. and A. Nakayama: Direct numerical simulation of open-channel flow with free-surface fluctuations, Journal of Hydraulic, Coastal and Environmental Engineering, JSCE, No.712/II-60, pp.57-72, 2002 (in Japanese).

APPENDIX – NOTATION

The following symbols are used in this paper:

$a_m(t_p)$ = modal amplitude (or modal time-series) as defined by Eq. (4);
B = channel width;
B/H = aspect ratio of channel;
C_m = cumulative contribution ratio as defined by Eq. (5);
$COR_{fg}(x, y)$ = space correlation coefficient of $f(t_p)$ and $g(x, y, t_p)$ as defined by Eq (6);
Fr = Froude number based on $\overline{U}$ and H $(\overline{U}/\sqrt{gH})$;
Fr_* = Froude number based on U_* and H $(u_*/\sqrt{gH})$;
$f(t_p)$ = fluctuation;
$g(x, y, t_p)$ = fluctuation;
g = gravitational acceleration;
H = mean water depth;

h = instantaneous water surface profile, $h = H + h'$;
h' = fluctuation component of the water surface profile;
h'_m = component of h' in POD mode m;
$\sqrt{\overline{h'^2}}$ = intensity of water surface fluctuations;
$\overline{h'^2_m}$ = mean square of water surface fluctuation h'_m;
i, j = integers;
k_m = wave-number of φ_m $(2\pi/L_m)$;
L_m = wavelength of φ_m;
L_m/H = non-dimensional wavelength;
M = total number of the discrete times;
m = number of the POD mode;
N = total number of the measurement points;
p'_{Lm} = pressure fluctuation with wavelength L_m;
Re = Reynolds number based on $\overline{U}$ and H $(\overline{U}H/\nu)$;
Re_* = Reynolds number based on U_* and H (U_*H/ν);
$[\mathbf{R}_h]=[\mathbf{R}_{i,j}]$ = covariance matrix of h' as defined by Eq. (2);
r_n = contribution ratio in each mode n;
t_p = discrete time;
$\overline{U}$ = mean bulk velocity;
U_* = friction velocity;
U^+ = mean velocity profile $(\overline{U}/U_*)$;
u'_{Lm} = turbulence with wavelength L_m;
U, V = components of mean velocity in the x-, y- directions, respectively;
u, v = instantaneous velocities in the x-, y- directions, respectively, $(u, v) = (U, V) + (u', v')$;
u', v' = velocity fluctuations in the x-, y- directions, respectively;
$\sqrt{\overline{u'^2}}$ = turbulence intensities in the x-directions;
$\sqrt{\overline{v'^2}}$ = turbulence intensities in the y- directions;
x_i = locations of each measurement point in the x-direction;
x, y = streamwise direction (positive downward) and vertical direction (positive upward), respectively, in the Cartesian coordinate with the origin at a point on the channel bed;
y^+ = vertical direction as the inner variable (yU_*/ν);
δ = thickness of the surface influence layer;
ν = kinematic viscosity;
κ = von Karman constant;
ρ = density of water;
φ_m = POD eigenvector as defined by Eq (1); and
λ_m = eigenvalue in POD mode m as defined by Eq (1).

(Received July 7, 2003 ; revised October 14, 2003)